River Flow 2010 - Dittrich, Koll, Aberle & Geisenhainer (eds) - © 2010 Bundesanstalt für Wasserbau ISBN 978-3-939230-00-7

Depth-averaged 2D models with effects of secondary currents for computation of flow at a channel confluence

Mung Dinh Thanh, I. Kimura & Y. Shimizu
Hydraulic Research Laboratory, Hokkaido University, Sapporo, Japan

T. Hosoda
Department of Urban Management, Kyoto University, Kyoto, Japan

ABSTRACT: Open-channel confluences are common in nature as well as in hydraulic structures, and play an important role in fluvial channel processes. The previous studies show that flow at the vicinity of a junction is characterized by three dimensionality and is affected by both turbulence and secondary currents of the first kind induced by curvature of the channel streamline. A 3D model enables to describe and compute most characteristics of flow in this region. However, such a model is still expensive and is not practical. Therefore, it should be useful and more practical if simpler models that enable to fairly well simulate flow at the junction are developed. For this purpose, we introduce some of such models, depth-averaged 2D models with effects of secondary currents of the first kind. By using these models, flow at the vicinity of the channel confluence is computed. In the present study, four different types of depth-averaged 2D models without and with effects of secondary current are performed. Model 1, which excludes effect of secondary current, is performed as a base case for comparison of the computed results of the three remaining others. Model 2 includes secondary current, while Model 3 considers not only this effect but also lag between the streamline and development of secondary current. Model 4, a more sophisticated one takes into account effects of secondary current, lag between the streamline curvature and development of secondary current, and the change of mainstream velocity profile caused by secondary currents. Computed results with these models are also compared to the experimental ones and to each other for discussion about adequacies of these models.

Keywords: Open channel flow, Secondary current, Depth-averaged 2D model

1 INTRODUCTION

Channel confluences are common in natural rivers as well as in hydraulic structures and are a fundamental morphological unit of channel and river networks. Flow features in these regions are complicated and are characterized with one separation zone or recirculation zone immediately downstream of the confluence in the inner bank side and one contracted flow region in the outer bank side. These features are influenced by numerous factors, such as geometry ones, for example, the size, shape, and slope of channels and angle between channels, and flow ones, for instance, the Froude number in the downstream flow, the ratio of discharge in the two channels. Complexity of flow at the vicinity of the junction arises due to deflection of lateral flow entering the main channel and this makes channel streamlines in the post-junction region curved. Recent 3D studies, such as Weber et al. (2001), Huang et al. (2002), Qing-Yuan et al.(2009), show that flow in a junction is three-dimensional with predominant secondary currents induced by curvature of the streamlines in comparison with the ones driven by turbulence. However, except for 3D computational models, normal 2D models do not usually include this flow pattern. Not considering secondary currents in modeling of these model leads to poor performance in cases where confluence flow is concerned.

Nowadays, development of computer technology provides powerful tools with them using three-dimensional (3D) models with millions of grid points in computing fluid dynamics is possible. However, application of the 3D models to practical problems with a large scale, such as flows at an open-channel network is difficult, because this system entails a combination of a main channel and some tributaries; typical examples are en-

countered in irrigation and drainage canals, urban water network, and natural river systems. 3D models, therefore, is usually used for very necessary cases where details of flow structure is paid attention. Moreover, using 3D computational models claims much labor and is costly.

For the reasons above, depth-averaged 2D models are still useful and more practical than 3D ones. In particular, depth-averaged 2D computational models considering effects of secondary currents are developed to predict flow in curved open channels. Several models of this kind proposed are ones of Kalkwijk & de Vriend (1980), of Hosoda et al. (2001) in which lag between main flows and secondary currents is included, and of Onda et al. (2006) with considering change of the velocity profile induced by development of secondary currents. The latter two have been recently paid attention and some studies applying these two models have been conducted. For instance, the work of Kimura et al. (2007) are based on applying these models to study features of flow and sediment transport in open-channel with a side cavity. An another application of these models was carried out by Kimura et al. (2009a) to study flow and sediment transport in meandering channels. Good performances were obtained in their studies. However, the literature does not indicate applicability of these models to simulate open-channel confluence flow.

The purpose of the present study, therefore, is to apply depth-averaged 2D models with effects of secondary currents for computation of flow in a vicinity of a channel confluence. In this study, four depth-averaged 2D models applied are

(a) Model 1: a conventional 2D model using a non-linear 0-equation turbulence model without effects of secondary currents;
(b) Model 2: a 2D model with effects of secondary current without consideration of lag between the streamline curvature and development of secondary currents;
(c) Model 3: a 2D model with effects of secondary currents and lag between the streamline curvature and development of secondary currents; and
(d) Model 4: a 2D model that consider effects of secondary currents, lag between the streamline curvature and development of secondary currents as well as change of mainstream velocity profile influenced by secondary currents.

Attempts to apply Model 2 are done during the process of implementation of this study, but are not successful. The reason for this may be attributed to very sharp streamline curvature of flow downstream of the junction causing very instability of this model. Therefore, in the following, only the results obtained from the models 1, 3 and 4 are reported.

Computational results are compared to experimental results of Weber et al. (2001). The present computed results show certain distinctions between using the depth-average models with effects of secondary currents and using the model without this consideration.

2 COMPUTATIONAL MODELS

2.1 *Fundamental equations*

The governing equations used in this study are depth-averaged 2D shallow water flow equations described in Kimura et al. (2007) in the Cartesian coordinate as follows.

Continuity equation:

$$\frac{\partial h}{\partial t}+\frac{\partial M}{\partial x}+\frac{\partial N}{\partial y}=0 \tag{1}$$

Momentum equations:

$$\begin{aligned}\frac{\partial M}{\partial t}+\frac{\partial \beta uM}{\partial x}+\frac{\partial \beta vN}{\partial y}+gh\frac{\partial (h+z_b)}{\partial x}=\\ gh\sin\theta-\frac{\tau_{bx}}{\rho}+\frac{\partial -\overline{u'^2}h}{\partial x}+\frac{\partial -\overline{u'v'}h}{\partial y}\\ +\nu\left\{\frac{\partial}{\partial x}\left(h\frac{\partial u}{\partial x}\right)+\frac{\partial}{\partial y}\left(h\frac{\partial u}{\partial y}\right)\right\}+S_{cx}\end{aligned} \tag{2}$$

$$\begin{aligned}\frac{\partial N}{\partial t}+\frac{\partial \beta uN}{\partial x}+\frac{\partial \beta vN}{\partial y}+gh\frac{\partial (h+z_b)}{\partial y}=\\ -\frac{\tau_{by}}{\rho}+\frac{\partial -\overline{v'u'}h}{\partial x}+\frac{\partial -\overline{v'^2}h}{\partial y}\\ +\nu\left\{\frac{\partial}{\partial x}\left(h\frac{\partial v}{\partial x}\right)+\frac{\partial}{\partial y}\left(h\frac{\partial v}{\partial y}\right)\right\}+S_{cy}\end{aligned} \tag{3}$$

where (x, y): spatial coordinate, (u, v): depth-averaged velocity components in (x, y) directions, t: time, h: water depth, (M, N): discharge fluxes in (x, y) directions defined as (hu, hv) respectively, g: gravity acceleration, (u', v'): turbulence velocities in (x, y) directions, z_b: bed level, (τ_{bx}, τ_{by}): bottom shear stress vectors, ν: dynamic viscosity coefficient, sinθ: bed slope, f: friction coefficient (function of Reynolds number), ρ: water density, β: momentum coefficient, $-\overline{u'^2}$,$-\overline{u'v'}$,$-\overline{v'^2}$: depth-averaged Reynolds stress tensors, and S_{cx} , S_{cy}: additional terms caused by secondary currents and defined later.

Components of the bottom shear stress vector are evaluated as

$$\tau_{bx}=\frac{f\rho u}{2}\sqrt{u^2+v^2};\quad \tau_{by}=\frac{f\rho v}{2}\sqrt{u^2+v^2} \tag{4}$$

in which, f: friction factor being a function of local Reynolds, $R_e' \equiv uh/\nu$, evaluated as follows.

$$f = \frac{6}{R_e'} \quad \text{for } R_e' \le 430 \tag{5a}$$

$$\sqrt{\frac{2}{f}} = A_S - \frac{1}{\kappa}\left[1 - \ln\left(R_e' - \sqrt{\frac{2}{f}}\right)\right] \quad \text{for } R_e' \ge 430 \tag{5b}$$

where $\kappa = 0.41$, $A_S = 5.5$.

The depth-averaged Reynolds stress tensors are evaluated based on the 0-equation turbulence model, but a non-linear term proposed by Kimura et al. (2009b) is added to the Reynolds stress tensor as

$$-\overline{u_i u_j} = (D_h + \nu)S_{ij} - \frac{2}{3}k\delta_{ij} - \lambda_p \frac{h}{u_*} D_h \sum_{\beta=1}^{3} c_\beta \left(S_{\beta ij} - \frac{1}{3}S_{\beta\alpha\alpha}\delta_{ij}\right) + C_{ij}u_*^2 \qquad i, j = 1,2 \tag{6}$$

Here, $S_{\beta ij}$ is defined as

$$S_{1ij} = \frac{\partial U_i}{\partial x_\gamma}\frac{\partial U_j}{\partial x_\gamma} \tag{7a}$$

$$S_{2ij} = \frac{1}{2}\left(\frac{\partial U_\gamma}{\partial x_i}\frac{\partial U_j}{\partial x_\gamma} + \frac{\partial U_\gamma}{\partial x_j}\frac{\partial U_i}{\partial x_\gamma}\right) \tag{7b}$$

$$S_{3ij} = \frac{\partial U_\gamma}{\partial x_i}\frac{\partial U_\gamma}{\partial x_j} \tag{7c}$$

D_h is eddy viscosity and is evaluated based on an non-linear 0-equation turbulence model considering contribution of strain and spin as well as reduction of eddy viscosity near wall as

$$D_h = f_D c_D \alpha h u_* \tag{8}$$

k is depth-averaged turbulent kinetic energy evaluated by the empirical formula proposed by Nezu & Nakagawa (1993) as

$$k = 2.07u_*^2 \tag{9}$$

Here, u_* is local friction velocity ($\equiv \sqrt{f(u^2+v^2)}$); α is calibrated constant ($\alpha = 0.80$ is used in this study).

λ_p is a coefficient calculated using the approach of Kimura et al. (2009b) ($\lambda_p = 4.29$ in the present study).

f_D is an eddy viscosity dumping function and is evaluated as

$$f_D = 4\frac{y_w}{h}\left(1 - \frac{y_w}{h}\right) \text{ for } y_w \le \frac{h}{2} \tag{10a}$$

$$f_D = 1 \text{ for } y_w > \frac{h}{2} \tag{10b}$$

Here, y_w is wall distance and h is water depth.

c_D is the coefficient of eddy viscosity and is a function of strain and rotation parameters as follows

$$c_D = \frac{1 + c_{ns}S^2 + c_{n\Omega}\Omega^2}{1 + c_{ds}S^2 + c_{d\Omega}\Omega^2 + c_{ds\Omega}S\Omega + c_{ds1}S^4 + c_{d\Omega 1}\Omega^4 + c_{ds\Omega 1}S^2\Omega^2} \tag{11}$$

Here, S and Ω are strain and rotation parameters, respectively and defined as

$$S = \lambda_p \frac{h}{u_*}\sqrt{\frac{1}{2}S_{ij}S_{ij}}\,, \Omega = \lambda_p \frac{h}{u_*}\sqrt{\frac{1}{2}\Omega_{ij}\Omega_{ij}} \tag{12}$$

$$S_{ij} = \frac{\partial U_i}{\partial x_j} + \frac{\partial U_j}{\partial x_i}\,, \Omega_{ij} = \frac{\partial U_i}{\partial x_j} - \frac{\partial U_j}{\partial x_i} \tag{13}$$

c_{ns}, $c_{n\Omega}$, c_{ds}, $c_{d\Omega}$, $c_{ds\Omega}$, c_{ds1}, $c_{d\Omega 1}$, $c_{ds\Omega 1}$ are model constants and their values are 0.005, 0.0068, 0.008, 0.004, -0.003, 0.00005, 0.00005, and 0.00025, respectively (Ali et al. (2007)). c_β is the coefficient of the non-linear quadratic term and evaluated (Ali et al. (2007)) as

$$c_\beta = c_{\beta 0}\frac{1}{1 + m_{ds}S^2 + m_{d\Omega}\Omega^2} \tag{14}$$

where $c_{\beta 0}$ (C_{10}, C_{20}, C_{30}) is the model constant for c_β. m_{ds} and $m_{d\Omega}$ are model constants for c_β and are of 0.01 and 0.003, respectively.

The fourth term at the right-hand side of Eq. (6) represents the effect of anisotropy in an equilibrium state. This term is first introduced by Kimura et al. (2009b) with coefficients C_{ij} evaluated as follows

$$C_{xx} = 2.07(C_{30} - 2C_{10})/3 \tag{15a}$$

$$C_{yy} = 2.07(C_{10} + C_{30})/3 \tag{15b}$$

$$C_{xy} = 0 \tag{15c}$$

$$C_{10} = 0.40, C_{20} = 0, C_{30} = -0.13 \tag{16}$$

2.2 *Secondary current model*

The additional terms expressing effects of secondary currents, S_{cx} and S_{cy}, in the equations (2) and (3) are defined as

$$S_{cx} = C_{sn}\left[\frac{\partial \bar{u}_s A_n h \sin 2\theta}{\partial x} - \frac{\partial \bar{u}_s A_n h \cos 2\theta}{\partial y}\right] + C_{n2}\left[-\frac{\partial A_n^2 h \sin^2\theta}{\partial x} + \frac{\partial A_n^2 h \cos\theta \sin\theta}{\partial y}\right] \tag{17}$$

$$S_{cy} = C_{sn}\left[\frac{\partial \bar{u}_s A_n h\cos 2\theta}{\partial x} - \frac{\partial \bar{u}_s A_n h\sin 2\theta}{\partial y}\right] + C_{n2}\left[\frac{\partial A_n^2 h\sin\theta\cos\theta}{\partial x} - \frac{\partial A_n^2 h\cos^2\theta}{\partial y}\right] \quad (18)$$

where C_{sn} and C_{n2} are model coefficients defined by equation (19) and are derived by Hosoda et al. (2001) using velocity profiles proposed by Engelund (1974) in the longitudinal and transverse directions f_s and f_n respectively, as

$$C_{sn} = \int_0^1 f_s(\zeta) f_n(\zeta) d\zeta \,,\; C_{n2} = \int_0^1 f_n(\zeta)^2 d\zeta \quad (19)$$

$\bar{u}_s$ is depth-average velocity in the streamwise direction and is defined by equation (20).

$$u_s(\zeta) = \bar{u}_s f_s(\zeta) \quad (20)$$

Here, $u_s(\zeta)$ is streamwise velocity profile in the vertical direction.

The coefficient A_n means the magnitude of the secondary current and is defined as

$$u_n(\zeta) = A_n f_n(\zeta) \,,\; \zeta = \frac{z}{h} \quad (21)$$

Here, $u_n(\zeta)$ is transverse velocity profile in the vertical direction and z is the direction perpendicular to the bottom bed. In the model neglecting the lag between the streamline curvature and the development of the secondary current (Model 2), A_n is simply evaluated as

$$A_n = \frac{\bar{u}_s h}{R} \quad (22)$$

where R is curvature radius of the streamline. In the model proposed by Hosoda et al. (2001), which includes the lag between the streamline curvature and secondary current, A_n is evaluated based on the depth-averaged transport equation of vorticity as

$$\frac{\partial}{\partial t}\left((u_n)_s - (u_n)_b\right) + \frac{\partial}{\partial x}\left((u)_s(u_n)_s - (u)_b(u_n)_b\right) + \frac{\partial}{\partial y}\left((v)_s(u_n)_s - (v)_b(u_n)_b\right) - \frac{1}{R}\left(\left(u_s^2\right)_s - \left(u_s^2\right)_b\right) = \frac{\partial}{\partial z}\left(\frac{\tau_{zn}}{\rho}\right)_s - \frac{\partial}{\partial z}\left(\frac{\tau_{zn}}{\rho}\right)_b \quad (23)$$

$$(u_n)_s - (u_n)_b = \hat{\lambda} A_n \quad (24)$$

$$\hat{\lambda} = \frac{\bar{u}_s}{\beta u_*}\frac{1}{\left(\frac{1}{3}+\beta r_*\right)^3}\left(\frac{1}{12}(\beta r_*)^2 + \frac{11}{360}(\beta r_*) + \frac{1}{504}\right) \quad (25)$$

$$r_* = \frac{\bar{u}_s}{u_*} - \frac{1}{3\beta} \quad (26)$$

Here, β is constant (=0.077) and $(u_s)_s$, $(u_s)_b$, $(u_n)_s$, $(u_n)_b$ are streamwise and transverse velocity at surface and bottom, respectively. u, v are same as ones in equations (2) and (3). In Model 4, A_n is evaluated as in Model 3, but the velocity profiles f_s and f_n are those derived by Onda et al. (2006) in which the important feedback mechanism between the main and secondary flow is considered. This feedback is attributed to the main reason causing deformation of vertical streamwise velocity profile, but it is not included in Model 2 and Model 3. A detail description of these models is given in Hosoda et al. (2001) and Onda et al. (2006).

2.3 *Computational scheme*

The fundamental equations are solved numerically using the finite volume method with a full staggered grid including conservativeness of physical quantities and computational stability. The QUICK scheme with second order accuracy in space is employed for convective inertia terms. The Adams Bashforth method with second order accuracy in time is used for time integration.

2.4 *Computational domain and conditions*

The depth-averaged 2D models in the present study are applied to the open-channel confluence flow using the experimental data of Weber et al. (2001) for verification. In this experiment, the channel consists of a main channel of 21.946m in length and a branch channel of 3.658 m in length located 5.486m downstream of the entrance of the main channel. Both these channels have the same width (W) of 0.914m. The total combined flow discharge (Q_t) is 0.170m^3/s and the downstream water depth is held constant at 0.296m. With these conditions, the averaged downstream velocity is 0.628 m/s corresponding to a Froude number of 0.37. A total of six runs of the experiments were conducted for six various values of q^* defined as the ratio of the upstream main channel flow (Q_m) to the total flow (Q_t).

In the present study, q* = 0.25, that is, Q_m = 0.043 m^3/s and Q_b (branch discharge) = 0.127 m^3/s, is selected for computations because this is a case, which generates strong secondary current at the vicinity of the junction and is a challenge for simulating as well. In order to facilitate simulation, the length of the post-junction channel is shorten to 7W (6.398m), where the water depth is nearly constant (H_0 = 0.3054m), while other dimensions of the computational domain are sameas

the ones in the experiment. Downstream bulk velocity, U_0, is approximate to 0.608 m/s.

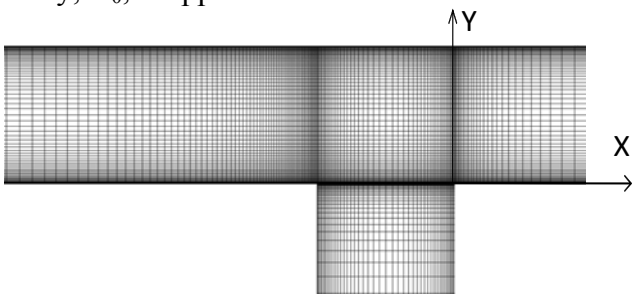

Figure 1. Computational grid around the confluence

The stretching grid is used in this study with the number of grid cells of 205 in the x-direction and 150 in the y-direction. The computational grid around the confluence is shown in Figure 1.

3 RESULTS AND DISCUSSIONS

3.1 *Velocity vector field and flow pattern*

In this study, all distances are normalized by the channel width, named as x/W, y/W. The velocity components are normalized by the downstream average velocity, U_0, called as u^* and v^* for u/ U_0 and v/ U_0, respectively. The u^*-v^* vector field calculated is compared with that observed in the experiment, but some preceding manipulations are done based on the experimental data to generate a depth-averaged one. The computational results are averaged between the 300th and 450th seconds. The experimental result is shown together with the computed ones as seen in Figure 2.

As seen from Figure 2, all three models reproduce important flow patterns at the vicinity of the junction, that is, a separation zone immediately downstream of the junction and a contracted flow with higher velocity. However, it can be seen that there is a difference in separation generated by Model 1 and by the others. Model 1 significantly under-predicts the length of this area, while both Model 3 and Model 4 fairly well reproduce it. It is supposed that the secondary current has an effect to extend the size of recirculation zone, because the flow near the bottom faces toward the center of this region and the reaction force acts enlarging the recirculation zone toward the outer side. Model 1 could not capture this effect, because it excludes the effect of the secondary current. Hence, the separation zone produced with Model 1 should be less than that obtained with Model 3 and Model 4. This result seems to be agreeable to guess of Cheng et al. (1992). On the contrary, Model 3 and 4 directly consider the effects of secondary currents. Therefore, the results calculated with these models are significantly improved in comparison with that with Model 1 and agree fairly well with the experimental one.

In addition, even though it is not presented here, an observation of process feature of the separation eddy shows that unsteady oscillation of the separation eddy can be seen in all results generated by the three models. This characteristic is appropriate to real phenomena.

However, as seen from Figure 2, all three models over-estimate velocity in the beginning reach of the separation where is adjacent to the junction. It may be due to the flow in this reach characterized with a highly three dimensionality, and a 2D model should not capture all flow features in spite of secondary current effects considered.

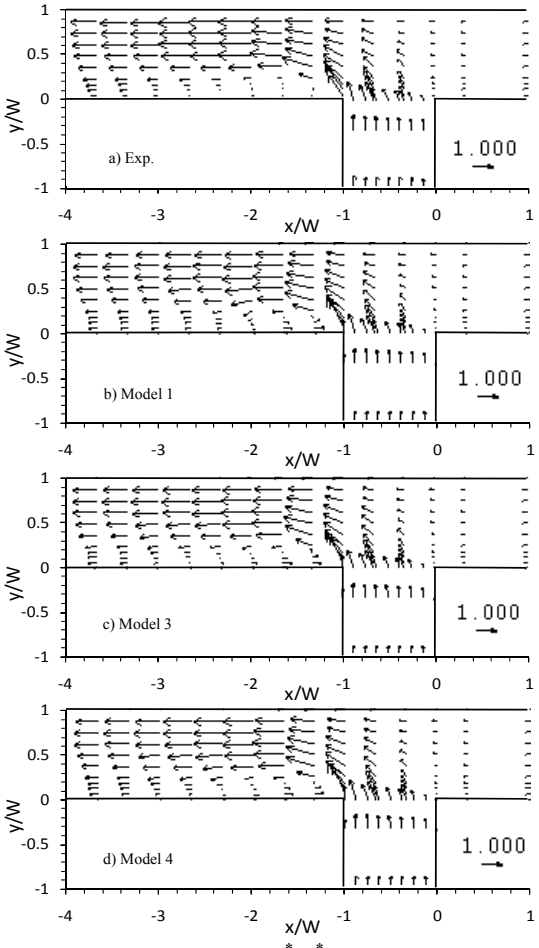

Figure 2. Comparison of u^*-v^* vector field.

3.2 *Velocity components*

In order to see more details of performances of the models, comparison of velocity profiles in the x- and y- direction is carried out. Figure 3 shows the streamwise velocity component profiles at some cross-sections along the post-confluence main channel, while Figure 4 depicts transverse ones at the same places. All velocity values are averaged over the depth. Positive values in Figure 3 indicate downstream motion, while negative ones show upstream motion.

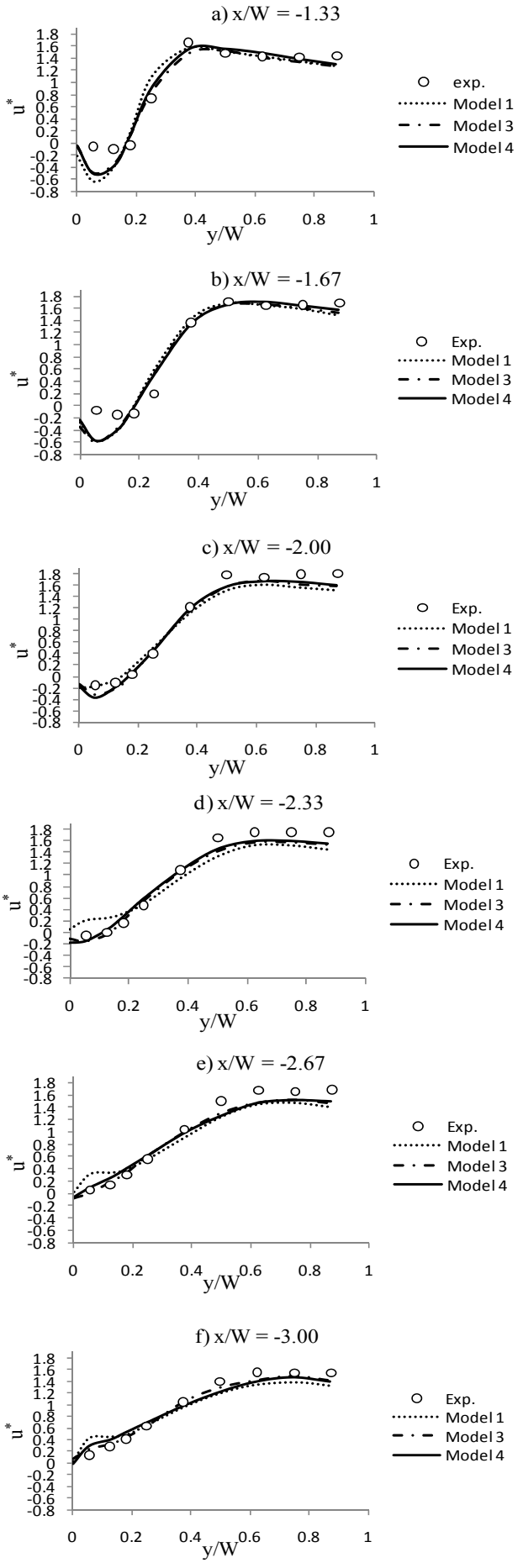

Figure 3. Comparison of longitudinal velocity component at some locations.

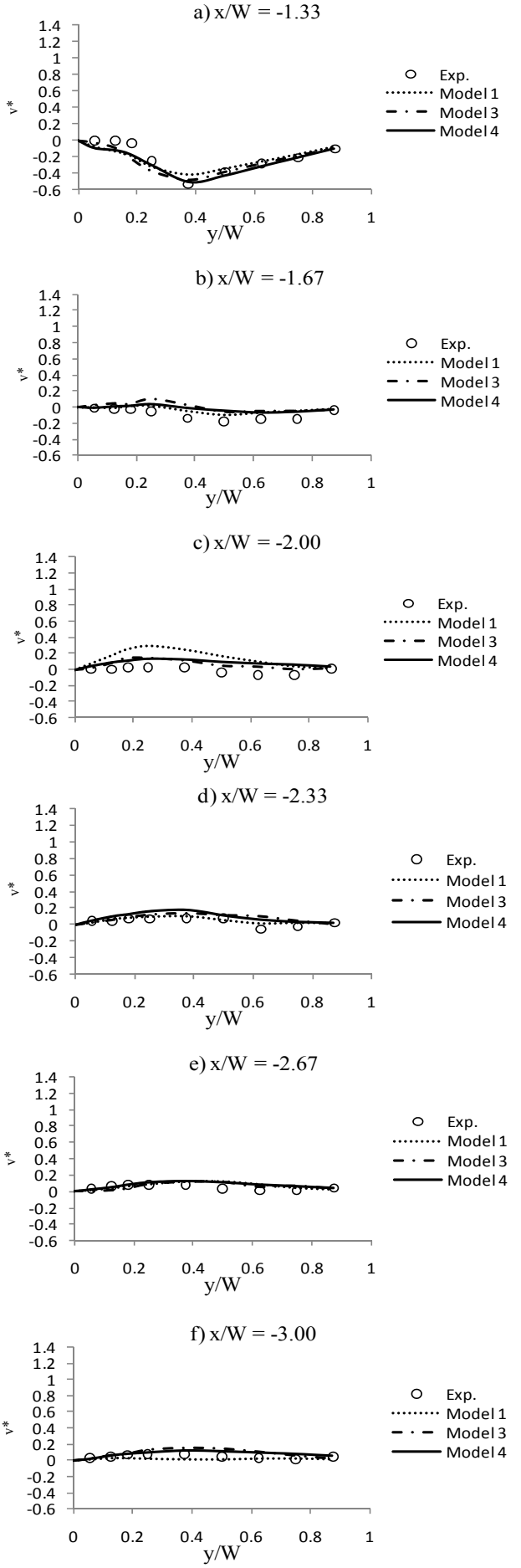

Figure 4. Comparison of cross-sectional velocity component at some locations.

It is observed in Figure 3, the results obtained with Model 3 and Model 4 agree well with the experimental ones, except for the beginning reach of the separation zone (In this reach, all models over-predict velocity as mentioned above). However, this similar agreement is not obtained with Model 1, because Model 1, as mentioned above, under-predicts the length of the separation zone. This can be seen in more details here. Figure 3 provides information on where the separation ends. As observed in Figure 3, the separation zone generated using Model 1 seems to drop after the section of x/W = -2.00 (exactly, x/W = -2.09), while it, in reality, extends to somewhere around the section of x/W=-2.67 as the experimental results and the ones obtained with Model 3 and Model 4. This can be realized, because velocity direction in the region near the inner bank of the main channel changes between the section of x/W=-2.00 and the section of x/W=-2.33 and the velocity profile in this region has a tendency to be flattened in the next sections as seen in Figures 3d, 3e and 3f. The reason for this shortcoming of Model 1, as explained above, is due to not considering adequately effects of secondary current. The result generated with Model 1 is hard to be accepted as a good prediction, because of the following reasons. First reason is that the separation zone itself is a region of reduced pressure and recirculating flow, and sediment tends to accumulate with consequences for hydraulic geometry, channel roughness, and so on. Hence, its size has effects on sediment deposition and confluence scour. Second one is that while secondary flow (helical flow) does not have strong influence on general flow pattern in rivers, it has a significant influence on the sediment transport direction and hence, morphological changes in the river channel (Olesen (1987)), and this flow is not included in Model 1. However, further researches, which apply the present models for calculation of sediment transport in a confluence, are necessary for confirmation of the above arguments.

Figure 4 shows profiles of dimensionless transverse velocity component at the same locations as in Figure 3. As shown from Figure 4, the transverse velocity component at most locations is much less than the longitudinal one, except for the section of x/W=-1.33. This distinction observed at the section of x/W=-1.33 is attributed to influence of flow coming from the branch channel. Models 3 and 4 provide the results agreeing with the measured one for all the locations, while Model 1 significantly over-predicts the transverse velocity component at x/W = -2.00 where the recirculating zone produced with Model 1 nearly ends, as obviously seen in Figure 4c.

It is also seen that it is not clear to realize difference between the results obtained using Model 3 and Model 4 with a comparison of depth-averaged velocity components. This may be because secondary current has a stronger effect on vertical mainstream velocity profile than on depth-averaged mainstream velocity one.

3.3 *Water surface elevation*

In this section, the results of water surface elevation, which is normalized by the channel width (W), predicted with the models are compared to the experimental one. Figure 5 shows the contours of measured and predicted dimensionless water surface elevations by Weber et al. (2001) and by using Models 1, 3 and 4, respectively. As known, one of distinctive characteristics of a sharp-edged, open-channel junction flow is an increase in depth from the downstream channel to the upstream contributing channels. This important feature is captured in all predicted results of water surface elevation with the models (as shown in Figures 5b, 4c, and 5d). In particular, all predict a rise of water surface level in the confluence region and this prediction for this area agrees well with the measured one. This implies practical applications for prediction of rise of water level caused by flood in confluence areas. The agreement between prediction of water level in the downstream of the separation zone with Model 4 and experiment is fair and reasonable, even though water surface elevation in the downstream of the separation is under-predicted a little bit and the trend of computed contours slightly departs from the experimental ones. However, the result with Model 1 for this region is disagreeable with the experimental one, and that with Model 3 seems quite unstable.

As can be seen in Figures 5c and 5d, difference in prediction of water surface elevation between the Model 4 and Model 3 is more obvious than that with the comparison of depth-averaged velocity profiles in the previous section. Model 4 generates the better result and more stable water level in the downstream of the separation than does Model 3. The reason for this may be explained as follows. Model 4 includes the feedback between the main flow and the secondary one, which is not considered in Model 3. While this feedback increases the main velocity component in the bottom region, it reduces this velocity in the surface one, thus causing a decrease in the flow momentum. This may lead to a stability of water surface with Model 4.

In summary, Model 4 performs a reasonable prediction of water surface elevation in comparison with the experimental one and much better than do the remaining two models, despite slight

disagreement with the experimental one for prediction in the downstream of the separation.

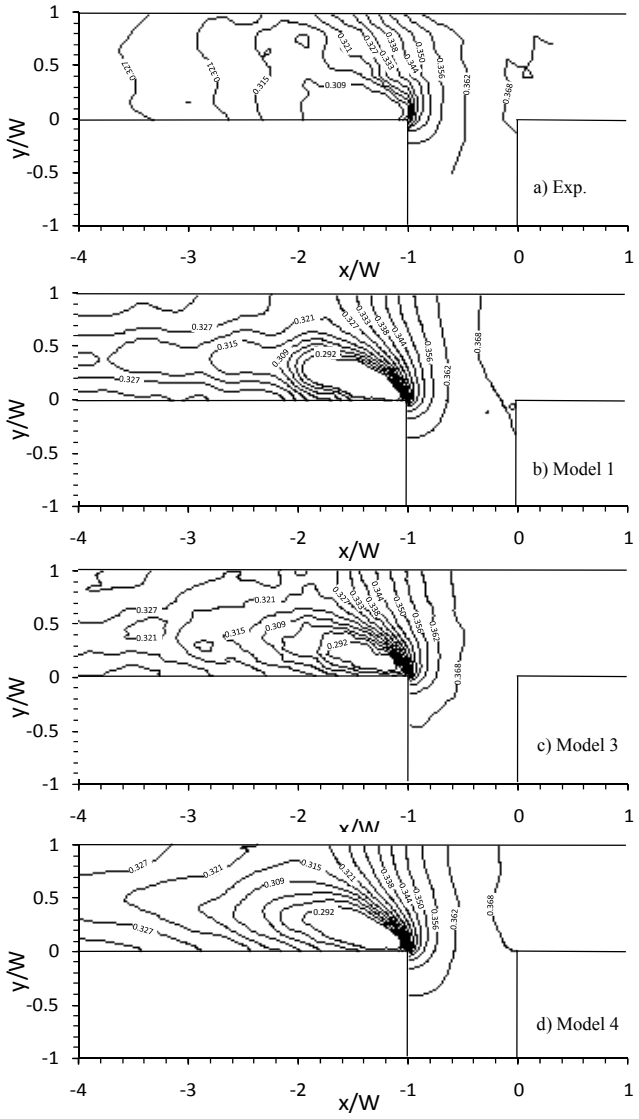

Figure 5. Comparison of water surface mappings.

4 CONCLUSION

In this study, four different types of depth-averaged 2D models with and without considering secondary currents are first applied to open-channel confluence flow. The most distinctive features of a sharp-edge open-channel junction are captured by using the present depth-averaged 2D models. In particular, Model 4 is the best one for-prediction of confluence flow, except for a small disagreement with the experimental result for computation of water surface elevation in the downstream of the separation. This indicates high applicability of the depth-averaged 2D models with effect of secondary current (Model 3 and Model 4) to an open-channel confluence flow in practice. The study also demonstrates failure of Model 2 in application to sharp-edged, open-channel confluence with a large junction angle. However, further applications of these models for computation of other problems, such as sediment transport, in this region are necessary for confirmation of their applicability in real cases.

REFERENCES

Ali, M. S., Hosoda, T., and Kimura, I. 2007. A non-linear k-ε model to predict the spatial change of turbulence structures in large scale vortices. Journal of Applied Mechanics, JSCE, Vol.10, 723-732.

Blankaert, K. 2002. Flow and turbulence in sharp open-channel bends. PhD-thesis. Ecole Polytechnique Federale de Lausanne.

Cheng, L., Komura, S., and Fujita, I. 1992. Numerical simulation of the confluence flow by using k-ε models. *Ann. J. Hydrau. Engrg, JSCE*, Vol.36, 169–174.

Engelund, F. 1974. Flow and bed topography in channel bends. *Proc, ASCE, J. Hydraulic Div.*, Vol.100, HY11, 1631-1648.

Hosoda, T., Nagata, N., Kimura, I., Michibata, K., and Iwata, M. 2001. A depth-averaged model of open channel flows with lag between main flows and secondary currents in a generalized curvilinear coordinate system. *Advances in Fluid Modeling & Turbulence Measurements*, (eds. H. Ninokata, A Wada and N. Tanaka), World Scientific, 63-70.

Huang, J., Weber, L. J., and Lai, Y. G. 2002. Three-dimensional numerical study of flows in open-channel junctions. J. Hydraul. Eng., Vol. 128(3), 268-280.

Kalkwijk, J. P. and De Vriend, H. J. 1980. Computational of the flow in shallow river bends. *J. Hydraulic Re.*, IAHR, Vol.18(4), 327-342.

Kimura, I., Hosoda, T., and Onda, S. 2007. Fundamental properties of suspended sediment transport in open channel flows with a side cavity. Proceedings of RCEM 2007, Enschede, Netherlands, Balkema Pblishers, 1203-1210.

Kimura, I., Onda, S., Hosoda, T., Shimizu, Y., and Hagiwara, K. 2009a. Computations of suspended sediment transport in meandering channels using depth-averaged models with effects of secondary currents. Proceedings of RCEM 2009, Santa Fe, Agentina, Balkema Pblishers, 619-626.

Kimura, I., Uijttewaal, W. S. J., Hosoda, T., and Ali, M. S. 2009b. URANS Computations of shallow grid turbulence. J. Hydraul. Eng., Vol.135(2), 118-131.

Masujin, K. and Shimizu, Y. 2005. Study on flow at a river confluence. Proceedings of RCEM 2005, Illinois, USA, Balkema Pblishers, 395-400.

Nezu, I. and Nakagawa, H. 1993. Turbulence in open-channel flows. IAHR Monograph, Balkema, Rotterdam, Netherlands.

Onda, S., Hosoda, T., and Kimura, I. 2006. Refinement of a depth-averaged model in curved channel in generalized curvilinear coordinate system and its verification. Ann. J. Hydrau. Engrg, JSCE, Vol.50, 769–774.

Quing-Yuan, Y., Xian-Ye, W., Wei-Zhen, L., and Xie-Kang, W. 2009. Experimental study on characteristics of separation zone in confluence zones in rivers. J. Hydraul. Eng., Vol. 14(2), 166-171.

Weber, L. J., Eric, D. S., and Nicola, M. 2001. Experiments on flow at a 90^{o} open-channel junction. J. Hydraul. Eng., Vol.127(5), 340-350.